ELSEVIER

Journal of Controlled Release 83 (2002) 415–425

journal of controlled release

www.elsevier.com/locate/jconrel

Noninvasive monitoring of local drug release in a rabbit radiofrequency (RF) ablation model using X-ray computed tomography

Agata Szymanski-Exner[a], Nicholas T. Stowe[b], Roee S. Lazebnik[a], Kyle Salem[a], David L. Wilson[a], John R. Haaga[c], Jinming Gao[a,c,*]

[a]*Department of Biomedical Engineering, Case Western Reserve University, Cleveland, OH 44106, USA*
[b]*Department of Surgery, Case Western Reserve University School of Medicine, Cleveland, OH 44106, USA*
[c]*Department of Radiology, University Hospitals of Cleveland, Cleveland, OH 44106, USA*

Received 19 June 2002; accepted 7 August 2002

Abstract

In this study, X-ray computed tomography (CT) was utilized as a noninvasive method to directly examine local drug release kinetics in livers before and following radiofrequency thermal ablation. Iohexol, a CT contrast agent, was used as a drug-mimicking molecule. Release of iohexol in healthy and ablated rabbit livers over 48 h was quantified and correlated with the release profiles from phosphate-buffered saline (PBS) in vitro. The results show that iohexol release in ablated livers is significantly slower than both release in normal livers and in vitro. The time at which 50% of the drug was released ($t_{1/2}$) into ablated liver (20.6±5.9 h) was 1.7 times longer than in normal liver (12.1±5.4 h) and approximately two times longer than that in PBS (10.1±1.2 h). The slower release in ablated livers is a result of severe tissue damage inflicted by thermal ablation, as supported by histological examination. This data suggests that a noninvasive imaging method provides a superior measurement over in vitro release studies in accurately quantifying the local release kinetics of an agent in an altered physiological system in vivo. Because the development of a successful local drug therapy is dependent on the understanding of the agent release kinetics at the implantation site, the noninvasive data may be indispensable in effectively predicting the implant behavior in a physiological system.

Keywords: Iohexol; Local drug delivery; Pharmacokinetics; Radiofrequency ablation; X-ray CT; Rabbit model

1. Introduction

Rapid development of imaging techniques and interventional procedures has led to a multitude of exciting and unconventional opportunities for the minimally invasive treatment of solid tumors [1–4]. Stemming from the high number of unresectable tumor cases, image-guided thermal ablation has

*Corresponding author. Department of Biomedical Engineering, Case Western Reserve University, 10900 Euclid Avenue, Cleveland, OH 44106, USA. Tel.: +1-216-368-1083; fax: +1-216-368-4969.

E-mail address: jmg23@po.cwru.edu (J. Gao).

0168-3659/02/$ – see front matter
PII: S0168-3659(02)00216-X

emerged as the cutting-edge treatment of liver, pancreas and prostate cancers [5–10]. In this procedure, the percutaneous insertion of a needle electrode to the site of a tumor is guided by an imaging method such as CT or MRI. Electric current at radiofrequency is applied through the needle directly to the tumor, leading to increased temperature and coagulative necrosis [8–10]. This method has been widely documented and early clinical trials have shown it to be a promising treatment for hepatocellular carcinoma among others [7,11–14]. Studies have shown that although RF ablation is able to destroy the majority of tumor tissue, tumor recurrence has been reported in many cases due to the incomplete elimination of all the cancer cells. Factors such as peripheral cooling of the tumor by blood flow limit the volume of ablation, which may in turn lead to local tumor recurrence at the distal ablation boundary and a need for adjuvant chemotherapeutic treatments [8,15–19].

Our current research addresses this potential shortcoming with the development of a local chemotherapy for potential use in tumors that have been treated with RF ablation [20,21]. Direct intratumoral delivery of a drug has the potential to increase the efficiency of delivery and improve drug efficacy while minimizing the undesirable toxic side-effects usually associated with systemic chemotherapy. Local drug therapy has been studied extensively and is well documented for tissues such as the brain [22–26]. However, in the case of thermally ablated tissue, the local tissue structure and function has been drastically altered by cellular necrosis, and the resulting effect on drug pharmacokinetics in vivo has yet to be determined.

Here we report on the application of the CT method in examining the release kinetics of an agent from a polymer millirod into viable or thermally ablated rabbit livers. Application of the CT method in drug concentration measurement in live animals was validated previously by our group with excellent results [27,28]. We showed that concentration of a model agent inside millirods measured by CT agreed within 8% with that measured by UV–Vis following removal of the implants and extraction of remaining iohexol [27]. In this study, the polymer millirod consists of a biodegradable polymer matrix entrapping iohexol (Omnipaque®), a CT contrast agent. Iohexol was used as a model drug because of its excellent X-ray attenuation properties and low cost. The device was fabricated in the geometry of a cylindrical millirod to eventually allow minimally invasive implantation by a tissue biopsy needle under image-guidance. The present study provides valuable insight regarding the effect of RF ablation on the tissue structure and drug release kinetics. We tested the hypothesis that the tissue damage inflicted by the ablation procedure will have a significant effect on the drug release rate from the implant, and thus must be taken into account when designing the therapeutic system for its clinical application. X-ray computed tomography (CT) was utilized as a noninvasive method to directly examine local drug release kinetics in livers prior to and following radiofrequency thermal ablation.

2. Materials and methods

2.1. Materials

Poly(D,L-lactide-*co*-glycolide) (PLGA, lactide: glycolide=1:1, 0.65 dl/g inherent viscosity) was purchased from Birmingham Polymers (Birmingham, AL). Iohexol (Omnipaque®, MW 821.14, 46.4% iodine) was purchased from Nycomed Amersham Imaging (Oslo, Norway) and poly(vinyl alcohol) (PVA, 13–23 kDa) was purchased from Aldrich (Milwaukee, WI). D(+)-Glucose was purchased from Fluka (Milwaukee, WI). Phosphate-buffered saline (PBS) and methylene chloride were obtained from Fisher Scientific (Pittsburgh, PA). Teflon tubes were purchased from McMaster–Carr Supply Company (Cleveland, OH). New Zealand white rabbits were obtained from Covance (Princeton, NJ).

2.2. Implant fabrication and in vitro characterization

Millirod implants were fabricated according to a previously established compression–heat molding procedure [29]. Briefly, PLGA microspheres (~ 4 μm diameter) were mixed with iohexol powder (obtained from lyophilized iohexol solution) to form a uniform mixture, and D(+)-glucose was added to

the mixtures in order to expedite the rate of release. The homogeneously mixed powder was placed in a mold and compressed at 4.6×10^6 Pa at 90 °C for 2 h. The resulting cylindrical millirods have an average diameter of 1.65 mm and a loading density of 10% iohexol with 30% glucose (w/w).

The in vitro release of iohexol from the millirods was measured in PBS (pH 7.4) using a previously reported procedure [29]. Typically, segments of millirods (~8 mm in length) were submerged in 10 ml PBS and placed in an orbital shaker (New Brunswick Scientific, model C24) at 37 °C and 100 rpm agitation. At each sampling point, the millirod was removed from the vial and placed into 10 ml of fresh PBS. The retained sample was analyzed using a UV–Vis spectrophotometer (Hitachi, model U-3210). The Beer–Lambert law was used to calculate the iohexol concentration based on a previously determined extinction coefficient (34.8 ml/(mg.cm)) at the maximum absorption wavelength (245 nm) of iohexol. The average amount of iohexol remaining in the implants was calculated from this data and was standardized to the initial loading of iohexol. The initial concentration of iohexol was calculated based on the theoretical iohexol loading density (10%) and measured volume of each implant.

2.3. RF ablation and millirod implantation in rabbit livers

Animal procedures followed an approved protocol by the Institutional Animal Care and Use Committee at Case Western Reserve University. Male New Zealand white rabbits (3–3.5 kg) were anesthetized using xylazine (5 mg/kg), acepromazine (2 mg/kg), atropine (0.2 mg/kg) and ketamine (50 mg/kg), all given intramuscularly. The right or medial liver lobe was exposed through a small midline abdominal incision. In the animals undergoing ablation, the liver capsule of the medial lobe was first perforated with an 18-gauge hypodermic needle, and the liver tissue was ablated with a 19-gauge needle electrode (Radionics®, Burlington, MA 01803) at 90±3 °C for 3 min, following a previously established method [30]. After ablation, millirods (7–8 mm in length) with 10% iohexol and 30% glucose were implanted into the ablated lobes. The right lobe in all the rabbits was exposed and perforated with an 18-gauge hypodermic needle. Millirods of the same composition used in the ablated lobe were implanted into non-ablated liver lobe for comparison. After implantation, a small piece of fat was removed from the animal and sutured on top of the implantation site to seal the wound and prevent the implant from slipping out. The abdomen was closed. Buprenex (0.03 mg/kg) and 30 ml of 0.9% saline (SQ) were given prior to recovery. The rabbits remained sedated with incremental administration of ketamine (25 mg/kg) on the day of surgery, so that the appropriate CT scans could be acquired. In preparation for the subsequent scans, xylazine (5 mg/kg) and ketamine (50 mg/kg) were used to sedate the animals.

2.4. CT monitoring and quantitative image analysis of iohexol release in vivo

Image acquisition parameters obtained from prior optimization studies (600 mAs, 120 kVp, 1 mm slice thickness) [27] were used to monitor the in vivo release kinetics of iohexol. Each rabbit was positioned in the scanner so that the scan plane was approximately perpendicular to the long axis of the millirod. The same position was maintained throughout the study. The first image series was taken at approximately 1 h following implantation. The subsequent time points were approximately 4, 24 and 48 h following implantation. This time varied somewhat between animals (a discrepancy of 15–30 min), and the actual time values were used during data analysis. After this period, the rabbits were sacrificed with an overdose of sodium pentobarbital, and the millirods were retrieved from the livers. The livers were removed and stored at −80 °C for histology analysis.

Quantitative image analysis follows a previously established procedure [27]. First, a three-dimensional registration method was used to spatially align serial CT volumes [28,31,32]. After registration, an image volume was created and re-sliced perpendicular to the long axis of the millirod. Slices were analyzed with ImageJ for the average change of intensity within the implanted rod. The measurement of agent concentration from the image data was carried out by taking the average pixel value measurements in circular regions of interest along the entire volume of the rod. Because the boundary of the implant is not clearly defined on the CT images due to inherent

properties of the imaging technique, we determined the center of the implant to be the maximum pixel value in the 5-pixel region of interest. Because the diameter of the implant was approximately 1.6 mm and the pixel size was 0.3125 mm, a diameter of 5 pixels (or 1.56 mm) was used to approximate the boundary. The amount of iohexol remaining in the implant was calculated by averaging the pixel values (in Hounsfield units) from the regions of interest within the millirod body, subtracting the average base polymer attenuation levels from the average data, and using a conversion factor of 8.46 HU/(mg/ml) to calculate concentration values [27]. The correction for respiratory motion was also applied to the data. This factor was determined from preceding studies comparing CT scans in the same rabbits before and after sacrifice. The 50% release time was calculated from exponential decay curves ($y = a \cdot e^{-bx}$) fit to the animal data and for the in vitro data by linear extrapolation between the 8 and 11-h points. The average release rate during each sampling interval was calculated by determining the slope of a line between each interval.

2.5. Histological analysis

All liver samples underwent gross histological examination and microscopic analysis. The diameter of the visible ablated area perpendicular to the ablation needle tract was measured three times and an average measurement of the ablation area was calculated. Representative sections of the specimens were removed and fixed in 10% formalin solution. The preserved sections were embedded in paraffin, sectioned into 5 μm slices and stained with hematoxylin and eosin (H&E). The H&E sections were examined to determine the normal tissue structure surrounding the implanted millirod and the damage inflicted by the implantation trauma and thermal ablation.

3. Results

3.1. In vivo characterization of local iohexol release in normal and ablated livers

Using our millirods with 10% iohexol and 30% glucose and optimal imaging parameters, we examined the release kinetics of iohexol from PLGA millirods in normal and ablated rabbit livers. CT was used to monitor the iohexol release in vivo over 48 h in the same animal ($n = 6$ in normal livers, $n = 4$ in ablated livers). Fig. 1A shows representative CT images of the iohexol millirods implanted in a normal and ablated lobe of the rabbit liver after 48 h. Qualitative examination shows that a higher amount of iohexol (more contrast) has been retained inside the PLGA millirods implanted in the ablated lobe (Fig. 1A right) than that in the normal liver lobe (Fig. 1A left). In addition, the zone of ablation is visible after 48 h (Fig. 1A right). Fig. 1B illustrates sets of representative surface plots that describe the CT intensity change in the millirod and the surrounding liver tissue over time. Based on the conversion factor (8.46 HU/(mg/ml) [27]), the CT intensity was converted to iohexol concentration to permit quantitative measurement of iohexol release in vivo.

Quantitative image analysis shows that the release of iohexol from the implants into normal livers is significantly faster than that into ablated livers (Fig. 2). The cumulative release is represented by the average concentration of iohexol remaining in the implant, which is the most direct measurement from the CT images. Table 1 summarizes these measurements for the five rabbits. It is important to note that R1 had no ablation, and instead had implants in two healthy liver lobes. The similar release profiles in both lobes in R1 indicate that the release is not dependent on the liver lobe in which it was implanted. Rabbits R2–R5 had one ablated lobe and one normal lobe, and significant differences can be noted in the release data at most time points. The iohexol concentration in the ablated liver implants is between 16 to 30% higher than that in the normal liver implants during the first hour and 15.2 to 81.7% higher in 12/16 time points. When examining the average measurements (Table 1) in the normal liver environment, approximately 20% less iohexol remains in the millirods after the first hour (107.9±8.9 mg/ml vs. 134.1±4.2 mg/ml in the ablated lobes). This discrepancy increases to 43% after 48 h. The 50% release time ($t_{1/2}$) differs significantly ($P = 0.046$) and is 1.7 times faster in normal liver (12.1±5.4 h) as compared to ablated liver (20.6±5.9 h). The release rate is significantly faster ($P = 0.01$)

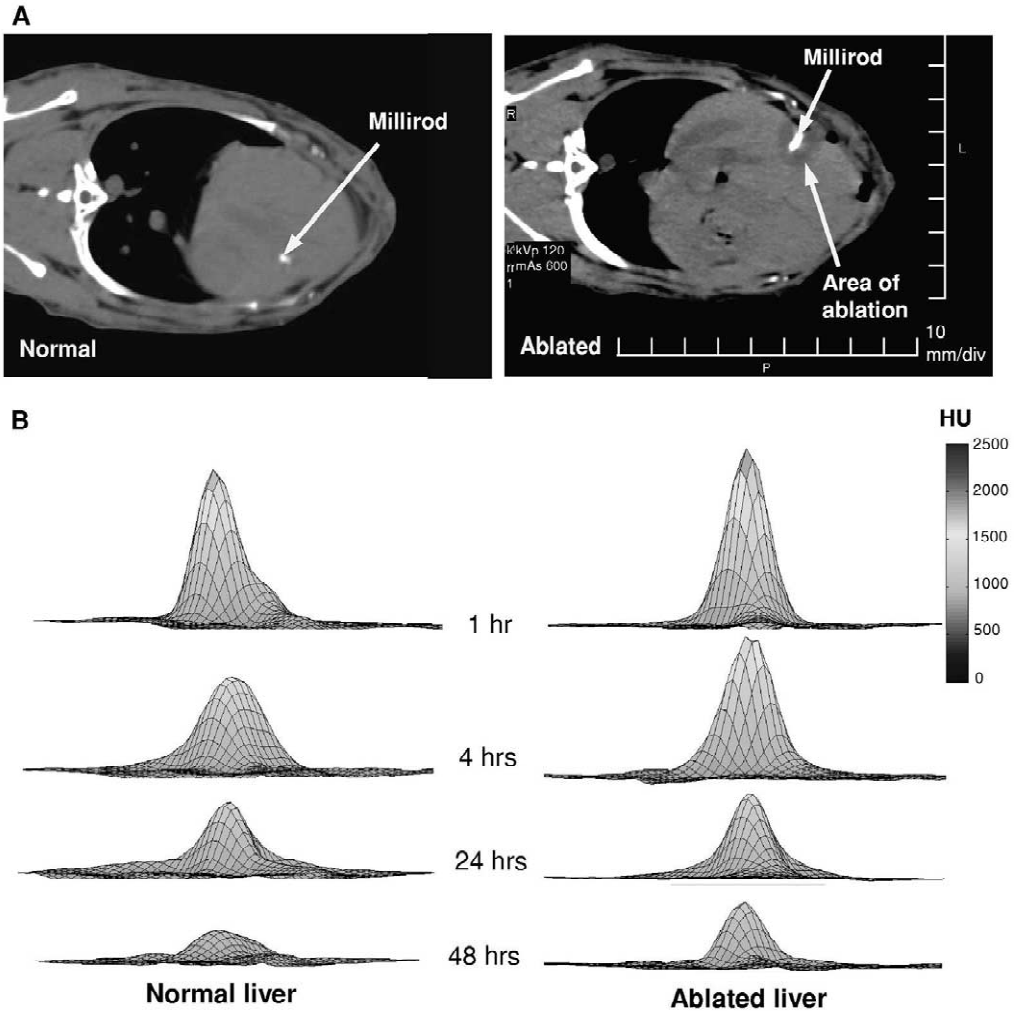

Fig. 1. Changes in the CT intensity reflect the rate of iohexol release from the millirod into normal and ablated livers. (A) Sample CT images showing a cross-section of a millirod (arrows) implanted in normal (left) and ablated (right) liver lobes after 48 h. The dark area surrounding the millirod in the ablated liver represents the area of ablation. Images were acquired at 120 kVp, 600 mAs and 1 mm slice thickness. (B) Surface plots showing the qualitative comparison of the CT intensity changes in millirods implanted in normal and ablated livers over time.

in the normal livers in the first hour (31.3±12.6 vs. 9.8±6.2 mg/ml/h in normal vs. ablated livers), but becomes comparable in both systems after 24 h (data not shown).

3.2. Variability of in vivo release kinetics between animals

We observed a high inter-animal variability in release kinetics among the five animals (see error bars in Fig. 2). When examining the difference between iohexol release in normal vs. ablated livers, a general trend of delayed release in ablated liver is apparent, and statistically significant differences from average normal liver release exist at the 1, 4, and 48 h points. The *P*-values calculated from an unpaired, two-tailed, Student's *t*-test were 0.001, 0.023 and 0.048, respectively. The *P*-value at the 24 h time point (0.19) is less significant, mostly due to the data variation between animals. The divergence

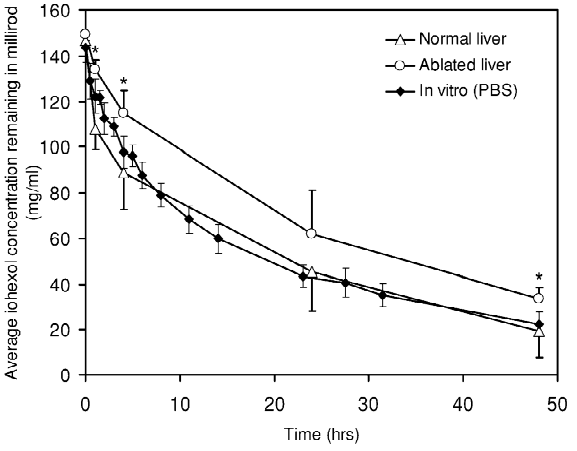

Fig. 2. Average cumulative release of iohexol from PLGA millirods in normal and ablated livers in vivo over 48 h. The in vitro release data in PBS at 37 °C is also shown for comparison. The error bars represent standard error, with portions of the bars omitted for clarity. Statistically significant differences (*$P<0.05$) were calculated by a two-tailed, unpaired Student's *t*-test and are between normal and ablated livers.

in release profiles between animals is clearly seen in Table 1. The variability ranges between ±4.2 to 19.4 mg/ml in the average in vivo release data. The in vivo variability is much greater than that in PBS in vitro, where the range is ±1.2 to 7.6 mg/ml for average release data. Despite individual variability, each rabbit showed consistently slower release kinetics in ablated livers over normal livers. These data demonstrate the advantage of CT as a noninvasive method of monitoring the sequential agent release in the same animal and using that animal as its own control to increase the sensitivity and accuracy of the pharmacokinetics studies.

3.3. In vitro/in vivo comparison of iohexol release

The in vitro release data were compared to those in vivo to evaluate the adequacy of the in vitro model in representing the physiological system (Fig. 2). The release of iohexol in vitro is comparable to that in normal livers, as evident by similar $t_{1/2}$ values. This indicates that the local release of an agent in normal livers is equivalent to, and therefore may be predicted by, the release in PBS. More specifically, the in vitro release predicts a $t_{1/2}$ of 10.1±1.2 h for normal livers and correlates well to the 12.1±5.4 h calculated from CT data (Table 1). The value of $t_{1/2}$ is two times longer in the ablated tissue (20.6±5.9 h) than indicated by the in vitro model. A similar trend is observed when examining the rate of release. Again, within the first hour, the in vitro release rate is comparable to that in normal

Table 1
Release profiles of iohexol in normal and ablated livers for all rabbits over 48 h

Rabbit	Liver	Iohexol remaining in millirod (mg/ml)					$t_{1/2}$
		0 h[a]	1 h	4 h	24 h	48 h	
R1	Normal	149.1	103.3	90.6	50.7	11.3	12.1
	Normal	149.1	115.5	86.4	45.1	9.4	11.2
R2	Normal	139.0	117.7	109.4	41.8	29.7	14.6
	Ablated	139.4	140.6	108.4	41.0	32.0	15.3
R3	Normal	155.5	110.2	69.1	37.2	31.2	10.6
	Ablated	157.0	131.3	104.2	58.8	30.8	18.8
R4	Normal	147.4	93.4	73.3	22.4	5.8	3.8
	Ablated	154.3	133.4	119.6	60.1	31.4	19.3
R5	Normal	141.1	107.6	104.9	74.5	28.2	20.4
	Ablated	147.3	131.6	126.2	87.9	41.0	29.1
Average	Normal	146.9±6.0	107.9±8.9[c]	88.9±16.2[c]	45.3±17.2	19.3±11.6[c]	12.1±5.4[c]
	Ablated	149.5±7.9	134.1±4.2	114.6±10.1	61.9±19.4	33.8±4.8	20.6±5.9
	In vitro[b]	143.7±6.7	122.2±7.6	97.7±7.0	43.4±4.9	22.3±5.4	10.1±1.2

[a] Initial concentration of iohexol was calculated based on the loading density of iohexol (10% w/w) and measured mass and volume of the implant.

[b] The in vitro release data was measured in PBS at 37 °C.

[c] Reflects a significant difference ($P<0.05$) between normal and ablated livers.

livers (21.5 vs. 29.1 mg/ml/h), but differs significantly from that in ablated liver (12.4 mg/ml/h). However, between 24 and 48 h, the rates are comparable in all three systems with 1.1, 1.2 and 0.84 mg/ml/h for normal, ablated and in vitro release, respectively.

3.4. Histological analysis

The gross morphology of the tissue surrounding the millirod was significantly altered in the ablated liver site (Fig. 3). The area affected by ablation was easily distinguished from the unaffected liver tissue. The tissue appeared dry with a tan color, and a hemorrhagic ring was visible at the distal edge of the ablated area. The calculated diameter of the ablated area ranged from 1.1 to 1.7 cm (1.4±0.2 cm). In comparison, the normal liver implantation site showed only a slight morphological change in the surrounding tissue, indicating an early response of the tissue to injury after 48 h.

Microscopic examination of the implantation site showed a vastly different tissue structure in the normal versus ablated liver tissue. The normal liver structure is shown in Fig. 4A, B. Hepatocytes are highly ordered in the hepatic lobule, around the sinusoids and the portal triad. The interstitial space is rather limited (Fig. 4A, B). In normal livers with implanted millirods, the implant-tissue interface showed slight signs of cellular damage due to the implantation trauma including a compressed cell shape, but no other signs of altered cellular architecture were visible (Fig. 4C, D). The morphology of the cells and vasculature next to the implantation was similar to that in the unaffected distal portion of the liver section. Some signs of hemorrhage can be identified as clusters of erythrocytes and inflammatory cells (Fig. 4D). In ablated livers, the tissue structure near the implantation site showed the same architecture as in the rest of the ablated area (Fig. 4E, F). The cellular structure was different from normal liver cells and corresponds to features of coagulative necrosis with pyknotic nuclei and disrupted and irregular cytoplasm. The sinusoidal structure was destroyed and the interstitial space was increased. At the distal edge of the ablated area, and at the interface of the ablated and normal liver tissue, a ring of inflammatory infiltrate, composed of lymphocytes and monocytes, was observed. Some signs of edema and hyperemia (increased blood flow to an

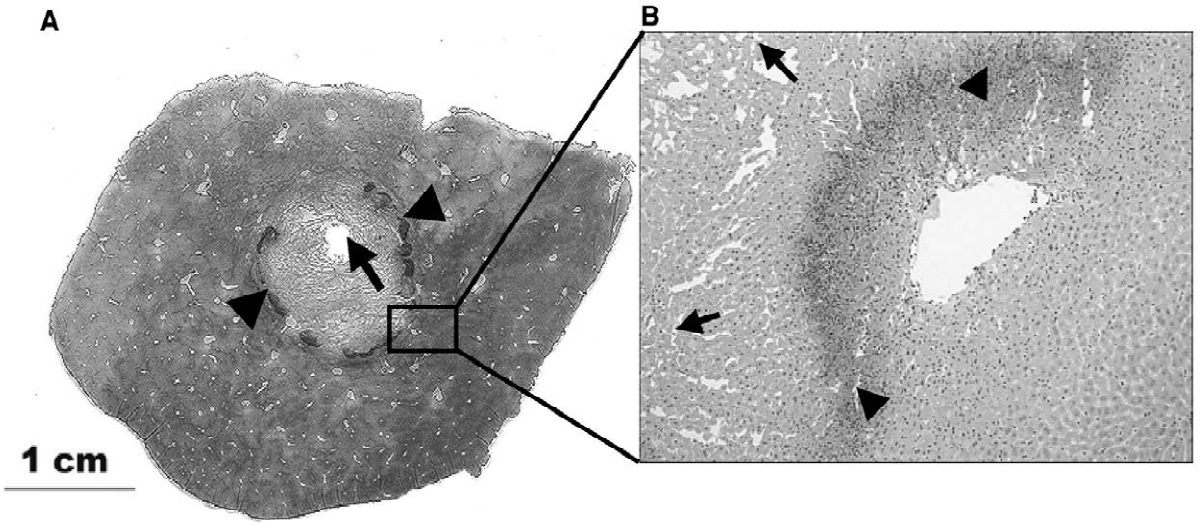

Fig. 3. Morphology of ablated rabbit livers after local delivery of iohexol for 48 h. (A) Gross examination of a 5 μm section of the ablated liver lobe. The millirod implantation site is visible in the center of the necrotic core (arrow). A ring of infiltrate resulting from the body's injury response is visible at the distal ablated tissue boundary (arrowheads). (B) The necrotic core (arrows) is characterized by increased interstitial space and disrupted vasculature. The infiltrate of monocytes and lymphocytes (arrowheads) is seen as the crescent-shaped front coming from the vein. The normal hepatocytes unaffected by the ablation are located at the bottom right corner (100×).

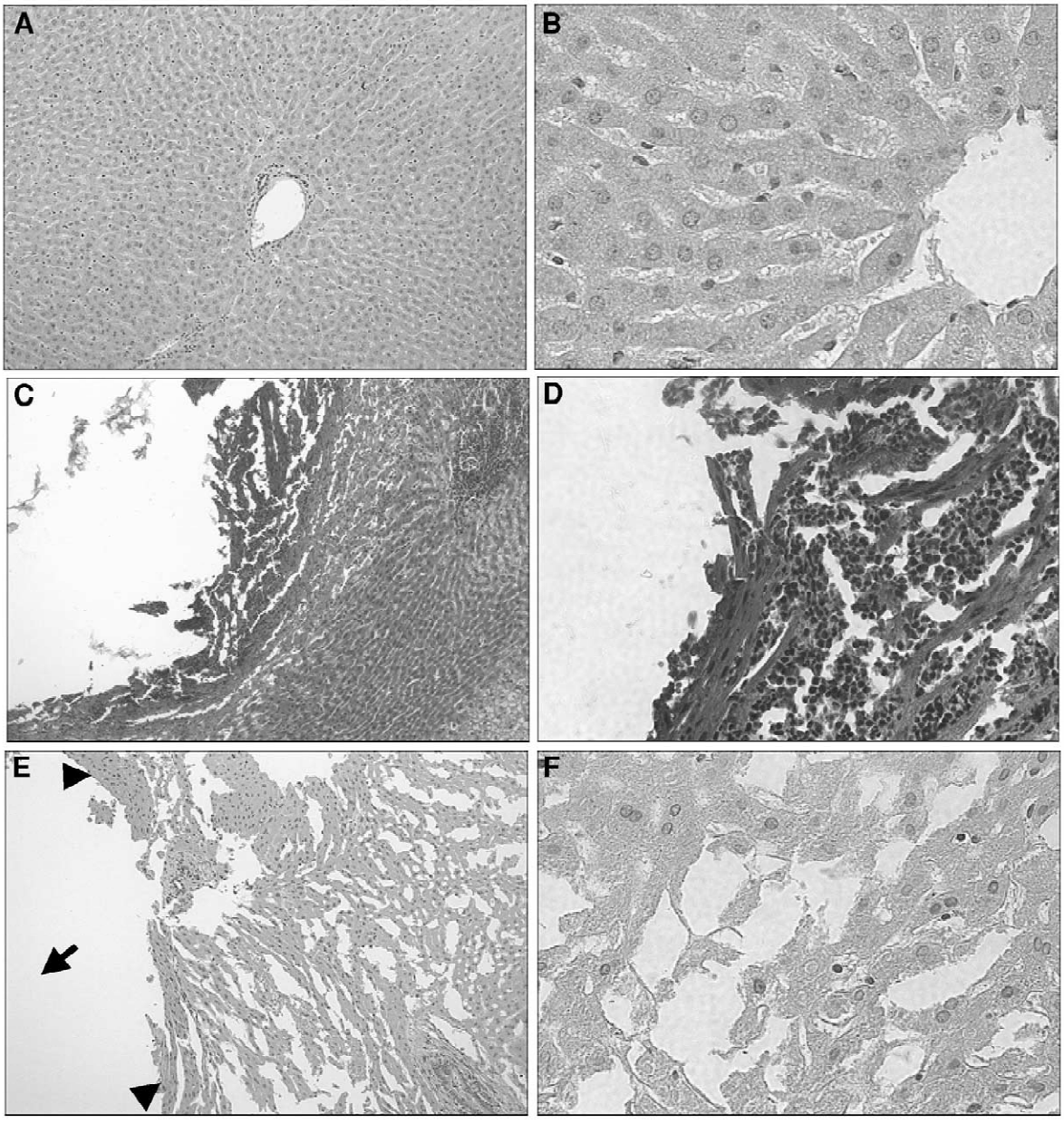

Fig. 4. Histological evaluation of the liver prior to and following RF ablation and millirod implantation. (A) Liver before implantation shows regular cellular architecture of a hepatic lobule. The portal triad is visible in the center and little or no interstitial space is present aside from the sinusoidal capillaries (100×). (B) Normal hepatocytes have round nuclei and roughly square cytoplasm (400×). Also seen is a portion of the central vein. (C) Implantation site in a non-ablated liver after 48 h. Cells adjacent to the implantation site appear compressed. A residual gathering of red blood cells (top middle) is indicative of a hemorrhage due to the implantation trauma (100×). (D) A magnified examination of the hemorrhage residue shows clusters of red cells at the implantation boundary. Also visible are monocytes and lymphocytes carried to the site as part of the wound healing response (400×). (E) Millirod implantation site in ablated liver after 48 h. The cells (arrowheads) adjacent to the implantation site (arrow) show an oblong morphology and appear necrotic (100×). (F) Destroyed cellular architecture resulting from ablation. Cellular necrosis can be classified by the pyknotic nuclei and disrupted cell membranes. Increased interstitial space and loss of sinusoidal structure is also visible (40×).

area), such as round inflamed hepatocytes and increased interstitial space, were also visible.

4. Discussion

The effect of tissue environment on drug release kinetics presents a unique challenge for the development of local drug delivery systems. Each tissue environment has a distinctive set of physiological parameters that affect the local release of a drug from the implant, and these effects must be evaluated before a successful local release system is produced. Here, we examined the influence of thermal ablation of the liver on the local drug release kinetics. Tissue damage caused by RF ablation is a chief factor in the potential clinical application of our drug delivery device.

The mechanism of iohexol release from the polymer millirods was adapted to suit the acute nature of the experiments. To meet the specific requirements for accurate and reproducible short-term release, we chose to use high loading densities of glucose (30%) to form interconnecting pores or channels in the polymer matrix upon water dissolution to facilitate the rapid release of iohexol. PLGA (50:50) was chosen for the polymer matrix because it is well characterized, and considered safe by the FDA for drug delivery applications [33]. Since the bulk degradation rate of the PLGA copolymer is rather slow (half-degradation time is 30 days), the fast iohexol release in 48 h is a result of diffusion from a multitude of pores and channels within the polymer matrix, not a result of PLGA degradation. The combined loading of iohexol and glucose (40%) is necessary to reach above the percolation threshold in the PLGA matrix to lead to a complete iohexol release [20].

Noninvasive examination of in vivo iohexol release from the millirods showed significantly slower release kinetics in ablated livers as compared to normal livers (Fig. 2, Table 1). We believe these results reflect the different drug transport processes at the two implantation sites. In normal livers, drug transport consists of interstitial diffusion, cellular uptake, and drug clearance by perfusion processes [34,35]. If iohexol, an extracellular contrast agent, is released into viable liver tissue, diffusion and perfusion are the only two processes taking place. In non-ablated livers, the clearance of iohexol from the tissue/implant interface is fast due to the high blood perfusion rate. Consequently, the release rate in normal livers is faster due to the higher concentration gradient at this interface.

In the ablated region, where the tissue is necrotic and the cells and vasculature have been destroyed, the dominant process of transport is through diffusion. Under such circumstances, iohexol concentration builds up at the tissue/implant interface, which hampers the release rate. The initial lag in iohexol release can be explained by the thermal injury inflicted on the liver. The cell necrosis and destruction of vasculature induced by the injury cause a drastic decrease in perfusion to the area. Immediately following the ablation, the area appears very dry, and this corresponds with the lack of dissolution and diffusion of iohexol from the implant. In the hours following ablation, as part of the inflammatory response, edema and hyperemia infiltrate the area, and once again allow for the release and diffusion of iohexol into the tissue. It should be noted that this fluid can play an important role in the latter stages of the release kinetics in the ablated liver site. Furthermore, because RF ablation increases the interstitial space for diffusion and reduces drug clearance due to perfusion, it is expected that the penetration and retention of a locally delivered drug in the ablated area should be greatly enhanced. This was demonstrated in a previous study where doxorubicin delivered to the ablated site remained in the area at therapeutic concentrations for over 24 h and penetrated the tissue to a depth of 5.2 mm, compared to 1.2 mm in the normal liver tissue [21].

The unique local environment of the ablated tissue requires special consideration for the development of a suitable local therapy. Test tube studies are widely accepted as a sufficient method to characterize the release kinetics of an agent from a drug delivery device. However, the current results suggest that precaution needs to be taken when in vitro release data is used to predict the release properties in vivo. In this study, although the in vitro model ($t_{1/2}$ = 10.1±1.2 h) agrees reasonably well with data from highly perfused normal liver tissues ($t_{1/2}$ = 12.1±5.4 h), we observed a two-fold increase in the release half-life in ablated liver tissue ($t_{1/2}$ = 20.6±5.9 h). In

the in vitro studies, iohexol released from the millirod is quickly dissolved and dispersed in the PBS buffer. Because of the relatively large volume of the buffer solution (10 ml per millirod) and frequent buffer change, the concentration gradient at the implant/solution interface is high, leading to release kinetics comparable to those in normal liver tissue. The discrepancy in release kinetics between PBS and ablated liver demonstrates the limitations of the PBS system in approximating drug release in ablated livers and the importance of noninvasive imaging techniques in pharmacokinetic studies.

5. Conclusions

Computed tomography was used to noninvasively monitor the release of a CT contrast agent (serving as a model drug) from a local drug delivery device into healthy and thermally ablated livers. It was found that iohexol release in ablated livers is significantly slower than that in normal livers, an observation correlating with the destruction of liver vasculature by thermal ablation. Importantly, the altered release profiles in ablated tissue cannot be accurately predicted by in vitro release data, demonstrating the limitations of in vitro analysis in implant characterization. These results clearly demonstrate the immense potential of using computed tomography in monitoring local pharmacokinetics and confirm that CT monitoring provides physiologically relevant data that may not be otherwise directly observed. Because of its noninvasive nature, the technique can examine release in the same animal over time and minimize the extensive sample collection and processing required with a large animal group compared to conventional pharmacokinetic methods. Future application of the CT method will provide fundamental knowledge in understanding drug transport in healthy and ablated liver tumor tissue in vivo, which will, in turn, permit rational design of millirods that will maximize the efficacy of local drug delivery following tumor RF ablation.

Acknowledgements

We would like to thank Les Ciancibello for his help with the CT image acquisition, Nancy Edgehouse for histological sample processing and Dr. James Anderson for his help in the histology analysis. Funding for this work was provided by the National Institutes of Health (R21 CA93993).

References

[1] G.J. Becker, 2000 RSNA annual oration in diagnostic radiology: the future of interventional radiology, Radiology 220 (2001) 281–292.
[2] C.E. Ray Jr., Interventional radiology in cancer patients, Am. Fam. Physician 62 (2000) 95–102.
[3] T.J. Vogl, P.K. Muller, M.G. Mack, R. Straub, K. Engelmann, P. Neuhaus, Liver metastases: interventional therapeutic techniques and results, Eur. Radiol. 9 (1999) 675–684.
[4] M.L. Montgomery, J.P. Sullivan, Advances in interventional radiology. The search for less invasive management sparks new approaches, Postgrad. Med. 109 (2001) 93–104.
[5] D.A. August, P.H. Sugarbaker, R.T. Ottow, Hepatic resection of colorectal metastases, Ann. Surg. 201 (1998) 210–218.
[6] S. Rossi, E. Buscarini, F. Garbagnati, M. Di Stasi, P. Quaretti, M. Rago, A. Zangrandi, S. Andreola, D. Silverman, L. Buscarini, Percutaneous treatment of small hepatic tumors by an expandable RF needle electrode, AJR Am. J. Roentgenol. 170 (4) (1998) 1015–1022.
[7] S. Rossi, M. Di Stasi, E. Buscarini, P. Quaretti, F. Garbagnati, L. Squassante, C.T. Paties, D.E. Silverman, L. Buscarini, Percutaneous RF interstitial thermal ablation in the treatment of hepatic cancer, AJR Am. J. Roentgenol. 167 (3) (1996) 759–768.
[8] L.R. Jiao, P.D. Hansen, R. Havlik, R.R. Mitry, M. Pignatelli, N. Habib, Clinical short-term results of radiofrequency ablation in primary and secondary liver tumors, Am. J. Surg. 177 (4) (1999) 303–306.
[9] J.S. Lewin, C.F. Connell, J. Duerk, Y. Chung, M. Clampitt, J. Spisak, G. Gazelle, J. Haaga, Interactive MRI-guided radiofrequency interstitial thermal ablation of abdominal tumors: clinical trial for evaluation of safety and feasibility, J. Magn. Reson. Imaging 8 (1998) 40–47.
[10] G.D. Dodd, M.C. Soulen, R.A. Kane, T. Livraghi, W.R. Lees, Y. Yamashita, A.R. Gillams, O.I. Karahan, H. Rhim, Minimally invasive treatment of malignant hepatic tumors: at the threshold of a major breakthrough, Radiographics 20 (1) (2000) 9–27.
[11] S.N. Goldberg, Radiofrequency tumor ablation: principles and techniques, Eur. J. Ultrasound 13 (2001) 129–147.
[12] S.N. Goldberg, G.S. Gazelle, C.C. Compton, P.R. Mueller, K.K. Tanabe, Treatment of intrahepatic malignancy with radiofrequency ablation: radiologic–pathologic correlation, Cancer 88 (2000) 2452–2463.
[13] T. Livraghi, S. Lazzaroni, F. Meloni, Radiofrequency thermal ablation of hepatocellular Carcinoma, Eur. J. Ultrasound. 13 (2001) 159–166.

[14] T. Yamasaki, F. Kurokawa, H. Shirahashi, N. Kusano, K. Hironaka, K. Okita, Percutaneous radiofrequency ablation therapy with combined angiography and computed tomography assistance for patients with hepatocellular carcinoma, Cancer 91 (2001) 1342–1348.
[15] C. Bartolozzi, L. Crocetti, D. Cioni, F.M. Donati, R. Lencioni, Assessment of therapeutic effect of liver tumor ablation procedures, Hepatogastroenterology 48 (38) (2001) 352–358.
[16] D. Cioni, R. Lencioni, C. Bartolozzi, Percutaneous ablation of liver malignancies: imaging evaluation of treatment response, Eur. J. Ultrasound. 13 (2) (2001) 73–93.
[17] R. Lencioni, O. Goletti, N. Armillotta, A. Paolicchi, M. Moretti, D. Cioni, F. Donati, A. Cicorelli, S. Ricci, M. Carrai, P.F. Conte, E. Cavina, C. Bartolozzi, Radio-frequency thermal ablation of liver metastases with a cooled-tip electrode needle: results of a pilot clinical trial, Eur. Radiol. 8 (7) (1998) 1205–1211.
[18] G. Francica, G. Marone, Ultrasound-guided percutaneous treatment of hepatocellular carcinoma by radiofrequency hyperthermia with a 'cooled-tip needle'. A preliminary clinical experience, Eur. J. Ultrasound 9 (2) (1999) 145–153.
[19] L. Buscarini, S. Rossi, Technology for radiofrequency thermal ablation of liver tumors, Semin. Laparosc. Surg. 4 (2) (1997) 96–110.
[20] F. Qian, N. Nasongkla, J. Gao, Membrane-encased polymer millirods for sustained release of 5-fluorouracil, J. Biomed. Mater. Res. 61 (2002) 203–211.
[21] J. Gao, F. Qian, A. Szymanski-Exner, N. Stowe, J. Haaga, In vivo drug distribution dynamics in thermoablated and normal rabbit livers from biodegradable polymers, J. Biomed. Mater. Res. 62 (2002) 308–314.
[22] M. Saltzman, in: Drug Delivery: Engineering Principles for Drug Therapy, Oxford University Press, 2001, pp. 235–315.
[23] L.K. Fung, M. Shin, B. Tyler, H. Brem, W.M. Saltzman, Chemotherapeutic drugs released from polymers: distribution of 1,3-bis(2-chloroethyl)-1-nitrosourea in the rat brain, Pharm. Res. 13 (5) (1996) 671–682.
[24] J.F. Strasser, L.K. Fung, S. Eller, S.A. Grossman, W.M. Saltzman, Distribution of 1,3-bis(2-chloroethyl)-1-nitrosourea and tracers in the rabbit brain after interstitial delivery by biodegradable polymer implants, J. Pharmacol. Exp. Ther. 275 (3) (1995) 1647–1655.
[25] R.L. Gutman, G. Peacock, D.R. Lu, Targeted drug delivery for brain cancer treatment, J. Controlled Release 65 (1–2) (2000) 31–41.
[26] H. Brem, H.C. Lawson, The development of new brain tumor therapy utilizing the local and sustained delivery of chemotherapeutic agents from biodegradable polymers, Cancer 86 (2) (1999) 325–330.
[27] A. Szymanski-Exner, N.T. Stowe, K.A. Salem, R.E. Lazebnik, J.R. Haaga, D.L. Wilson, J. Gao, Noninvasive monitoring of local drug release using X-ray computed tomography: optimization and in vivo/in vitro validation, J. Pharm. Sci. (2002) (in press).
[28] K.A. Salem, A. Szymanski-Exner, R.E. Lazebnik, M.S. Breen, J. Gao, D.L. Wilson, X-ray computed tomography methods for in vivo evaluation of local drug release systems, IEEE-Transact. Med. Imag. (2002) (in press).
[29] F. Qian, A. Szymanski, J. Gao, Fabrication and characterization of controlled release poly(D,L-lactide-co-glycolide) millirods, J. Biomed. Mater. Res. 55 (4) (2001) 512–522.
[30] E.M. Merkle, D.T. Boll, T. Boaz, J.L. Duerk, Y.C. Chung, G.H. Jacobs, M.E. Varnes, J.S. Lewin, MRI-guided radiofrequency thermal ablation of implanted VX2 liver tumors in a rabbit model: demonstration of feasibility at 0.2 T, Magn. Reson. Med. 42 (1) (1999) 141–149.
[31] R.S. Lazebnik, T.L. Lancaster, M.S. Breen, J.S. Lewin, D.L. Wilson, Volume registration using needle paths and point landmarks for evaluation of interventional MRI treatments, IEEE Transact. Med. Imag. (2001) (submitted for publications).
[32] R.S. Lazebnik, T.L. Lancaster, M.S. Breen, S.G. Nour, J.S. Lewin, D.L. Wilson, Volume registration of interventional MRI data using needle paths and point landmarks, in: Proceedings of SPIE Medical Imaging 2002: Visualization, Display, and Image-Guided Procedures, 2002.
[33] R.A. Jain, The manufacturing techniques of various drug loaded biodegradable poly(lactide-co-glycolide) (PLGA) devices, Biomaterials 21 (23) (2000) 2475–2490.
[34] R.K. Jain, Delivery of molecular and cellular medicine to solid tumors, J. Controlled Release 53 (1998) 49–67.
[35] J.L. Au, S.H. Jang, J. Zheng, C. Chen, S. Song, L. Hu, M.G. Wientjes, Determinants of drug delivery and transport to solid tumors, J. Controlled Release 74 (1–3) (2001) 31–46.